Electronic Supplementary Information

Electrochemical Nitrate Reduction for Ammonia Production: Amorphous or Crystal One?

Quanxiao Peng[a, b], Dandan Xing[b], Liuqi Dong[a], Yuhan Fu[a], Jixue Lu[a], Xiaoyu Wang[c]*, Changhong Wang[a]* and Chunxian Guo[a]*

[a] School of Materials Science and Engineering, Suzhou University of Science and Technology Suzhou 215011, P. R. China

[b] College of Chemistry, Chemical Engineering and Materials Science, Soochow University, Suzhou, 215123 P. R. China

[c] School of Physics and Optoelectronic Engineering, Hainan University, Haikou 570228, China.

* Corresponding Author: E-mail address: cxguo@usts.edu.cn; chwang@usts.edu.cn; xiaoyuwang@hainanu.edu.cn

Experimental Methods

Materials

Copper chloride dihydrate was purchased from Shanghai Aladdin Biochemical Technology Co., Ltd. Ethylene glycol, potassium hydroxide, Tannic acid, and polyvinyl pyrrolidone (K23-27) were purchased from Shanghai Titan Scientific Co., Ltd. Sodium borohydride and acetone were purchased from Sinopharm Chemical Reagent Co., Ltd. Carbon cloth (CR2032) was purchased from Pengxiang Yunda Machinery Technology Co., Ltd. All materials were purchased and used without further purification. In all experiments, deionized water with a conductivity of 18 MΩ was employed, following purification through a Millipore system.

Catalyst preparation

Preparation of a-O-Cu: 0.2 g of $CuCl_2 \cdot 2H_2O$ was dispersed in 40.0 mL of ethylene glycol to come into a stable solution by ultrasonication and stirring for 15 min. Afterward, 80.0 mg of tannic acid was added, and the solution was maintained in a uniform state through ultrasonication and stirring. Ultimately, 2.0 mL of 1 M KOH was dripped into the solution drop by drop, while stirring for an additional 5 minutes. The final product was collected by centrifuging, washed several times with acetone to ensure the absence of ethylene glycol in the sample, and then aggregated quantification to 10.0 mL with acetone. All these procedures were conducted at room temperature with stirring in air.

Preparation of c-O-Cu: 0.2 g of $CuCl_2 \cdot 2H_2O$ was dispersed in 35.0 mL of ethylene glycol to form a stable solution through ultrasonication and stirring for 15 minutes. Subsequently, 5.0 mL of 0.02 M PVP was added. After the solution was ultrasonicating and stirred for 5 min, 200.0 mg of $NaBH_4$ was rapidly added to the mixture under magnetic stirring, while stirring for an additional 5 minutes. The final product was collected by centrifuging, washed with acetone several times to make sure the absence of ethylene glycol in the sample, and then aggregated quantification to 4.0 mL with acetone. All these procedures were conducted at room temperature with stirring in air.

Catalyst characterization

X-ray diffraction (XRD) measurements were conducted using a Bruker D8 Advance powder XRD system equipped Cu Kα (λ = 1.54056 Å) radiation (50 kV, 200 mA) from the 2θ = 10 to 80° with a scanning speed of 4° min^{-1}. X-ray photoelectron spectroscopy (XPS) measurements were performed on a Thermo Fisher ESCALAB Xi+ instrument, employing non-monochromatized Al-K X-ray as the excitation source. The morphologies structures of the samples were observed via transmission electron microscopy (TEM) and selected area electron diffraction (SAED) by using Tecnai G2 F20 S-Twin (200 keV).

Electrocatalytic measurement of nitrate reduction.

The H-type electrochemical cell consisted of two chambers, namely, the anolyte and catholyte chambers, separated by a cation-exchange membrane known as the Nafion 117 membrane. In this configuration, both a-O-Cu and c-O-Cu were separately loaded onto carbon cloth substrates, each with a mass loading of 0.5 mg cm^{-2}. Within this setup, a saturated calomel reference electrode (SCE) was utilized as the reference electrode while a platinum foil measuring 1 × 1 cm^2 served as the counter electrode. The cathode

compartment's electrolyte was comprised of 1 M KOH, supplemented with 200 ppm NO_3^--N, and had a total volume of 40 mL. Conversely, the anode compartment's electrolyte consisted of 1 M KOH, also at a volume of 40 mL. Perform the linear sweep voltammetry with a scanning speed of 5 mV s^{-1}. Additionally, potentiostatic tests on the catalysts were carried out at various potentials, each lasting for 3 hours, with continuous stirring at a rate of 400 rpm.

For all the electrochemical tests conducted, the applied potentials were transformed into the reversible hydrogen electrode (RHE) scale according to the equation (1):

$$E_{RHE} = E_{SCE} + 0.241 + 0.059 \times pH \quad (1)$$

Detection method of ion concentration in electrolyte

The concentrations of NO_3^--N, nitrite-N (NO_2^--N), and ammonia-N (NH_4^+-N) were estimated using UV-Vis spectrophotometry following the standard method. Standard solutions of NO_3^--N, NO_2^--N, and NH_4^+-N were prepared to draw standard curves, respectively. The ion concentration in the electrolyte was measured before and after the experiment. First, dilute it to a suitable concentration. Then, use an UV-Vis spectrophotometer to measure its concentration. Finally, calculate the results by inputting the ion concentrations in the electrolyte measured before and after the experiment into their respective corresponding standard curves. The particular methods are as follows.

Determination of NO_3^--N: Dilute the electrolyte into 5 mL within the detection range and add 100 μL of 1 M HCl and 10 μL 0.8 wt% sulfamic acid solution. The absorption intensities at wavelengths of 200 nm and 275 nm were recorded. The absorbance value via the equation (2):

$$A = A_{220nm} - 2A_{275nm} \quad (2)$$

The concentration-absorption curve was obtained through a range of standard potassium nitrate solution measurements.

Determination of NO_2^--N: The nitrite color reagent is mixed phosphoric acid (10 mL, ρ = 1.70 g mL^{-1}), N-(1-Naphthyl) ethylenediamine dihydrochloride (0.2 g), p-aminobenzenesulfonamide (4 g), and DI water (50 mL). A set amount of electrolyte from the cell was diluted to a volume of 5 mL. Finally, add 100 μL of the color reagent to the 5 mL solution and mix thoroughly, allowing it to sit for 20 minutes. The absorption at a wavelength of 540 nm was recorded. The concentration-absorbance curve was calibrated through a range of standard sodium nitrite solutions.

Determination of NH_4^+-N: A given amount of electrolyte was diluted into a volume of 5 mL and added 100 μL 500 g L^{-1} potassium sodium tartrate solution and 150 μL of Nessler's reagent. Let the solution stand in the dark for 20 minutes. Record the absorption strength at a wavelength of 420 nm. Construct concentration-absorption curves using a range of standard ammonium chloride solutions.

Calculation of the NH_3 Faradaic efficiency and NH_3 selectivity

The Faradaic efficiency of NH_3 was calculated using the equation (3):

$$\text{Faradaic efficiency} = (n \times V \times C_{NH_3} \times F) / (M_N \times Q) \times 100\% \quad (3)$$

The NH_3 selectivity was obtained through the equation (4):

$$\text{Selectivity} = C_{NH_3} / \Delta C_{NO_3^-} \times 100\% \quad (4)$$

The NO_2^- selectivity was obtained through the equation (5):

Selectivity = $C_{NO_2^-}$ / $\Delta C_{NO_3^-}$ × 100% (5)

The yield of $NH_{3(aq)}$ was calculated through the geometric area of working electrode using the formula (6):

$Yield_{NH_3}$= (C_{NH_3}× V) / (M_{NH_3}× S × t) (6)

The yield of $NH_{3(aq)}$ was calculated through the loading mass of catalyst using the formula (7):

$Yield_{NH_3}$= (C_{NH_3}× V) / (M_{NH_3}× $M_{catal.}$ × t) (7)

where n denotes the number of electron transfers required for the production of 1 mole of ammonia, which is 8. V represents the volume of the catholyte, which is 40 mL. C_{NH_3} is the mass concentration of NH_3. $C_{NO_2^-}$ is the mass concentration of NO_2^-. F is Faraday constant (96485 C mol^{-1}). M_N represents the molar mass of N. Q signifies the total charge passing through the electrode. $\Delta C_{NO_3^-}$ represents the concentration change of NO_3^- before and after electrolysis. M_{NH_3} is the molar mass of NH_3. t is the electrolysis time (3 h). S is the geometric area of working electrode (1 cm^2). And $M_{catal.}$ is the loading mass of catalyst (0.5 mg).

DFT calculation

The density functional theory (DFT) calculations were performed using the Vienna Ab initio Simulation Package (VASP)[1, 2], with the generalized gradient approximation (GGA) Perdew–Burke–Ernzerhof (PBE) functional [3] to describe electron exchange and correlation. The projector-augmented plane wave (PAW) [4, 5] potentials were used to describe the core-valence electron interaction and take valence electrons into account using a plane wave basis set with a kinetic energy cutoff of 450 eV. The k points of Brillouin zone was set to be 3 × 4 × 1. Partial occupancies of the Kohn−Sham orbitals were allowed using the Gaussian smearing method and a width of 0.05 eV. The electronic energy was considered self-consistent when the energy change was smaller than 10^{-5} eV. A geometry optimization was considered convergent when the force change was smaller than 0.02 eV/Å.

For the amorphous oxidized copper, the structure was built by Ab initio molecular dynamics (AIMD) simulations via a traditional melted and quenched process.[6] For amorphous oxidized copper slab and crystalline oxidized copper slab model, a 15 Å vacuum layer was constructed to prevent the interaction between the periodic layers. For all surface calculations, the atoms in the bottom layer of the model were fixed and other atoms were allowed to move.

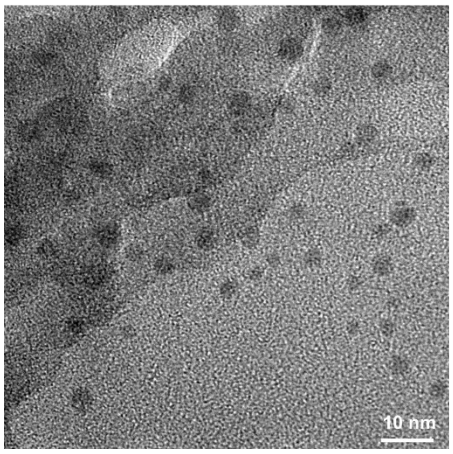

Figure S1. The TEM image of a-O-Cu.

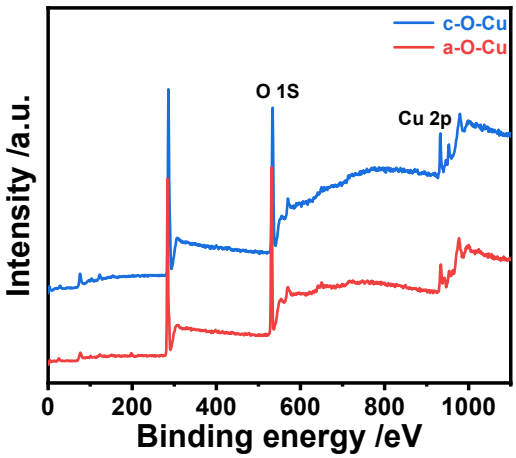

Figure S2. XPS survey spectra of c-O-Cu and a-O-Cu.

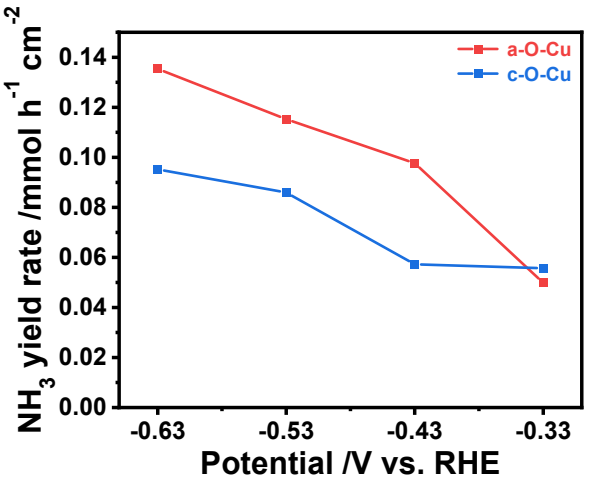

Figure S3. NH_3 yield rate of a-O-Cu and c-O-Cu at -0.63 V, -0.53 V, -0.43 V, and -0.33 V vs. RHE for 3 h.

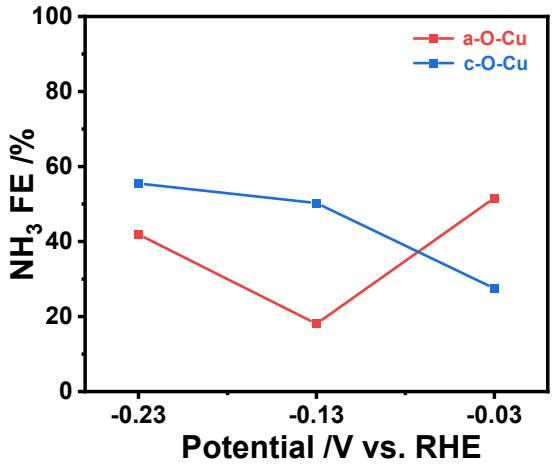

Figure S4. NH_3 FE of a-O-Cu and c-O-Cu at different potentials for 3 h.

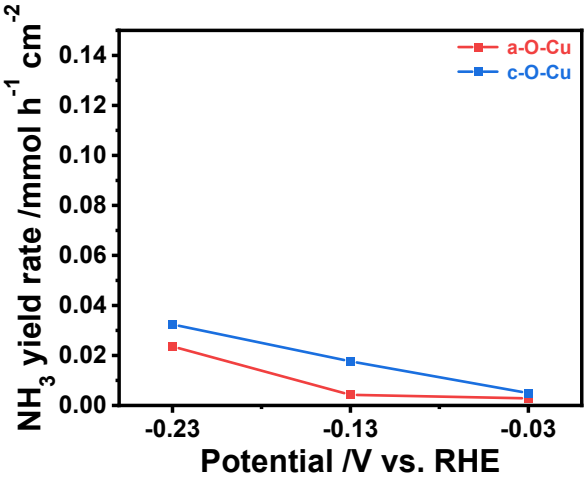

Figure S5. NH_3 yield rate of a-O-Cu and c-O-Cu at -0.23 V, -0.13 V, and -0.03 V vs. RHE for 3 h.

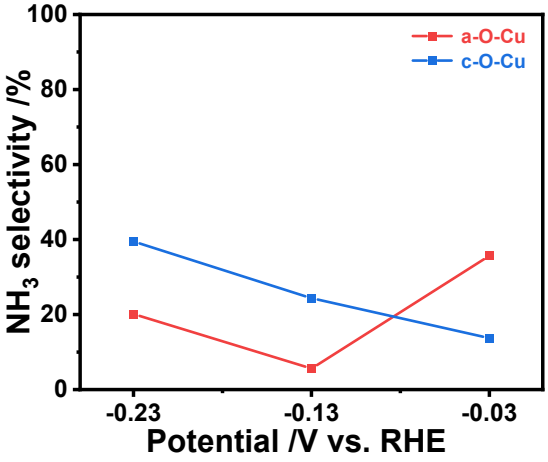

Figure S6. NH_3 selectivity of a-O-Cu and c-O-Cu at different potentials for 3 h.

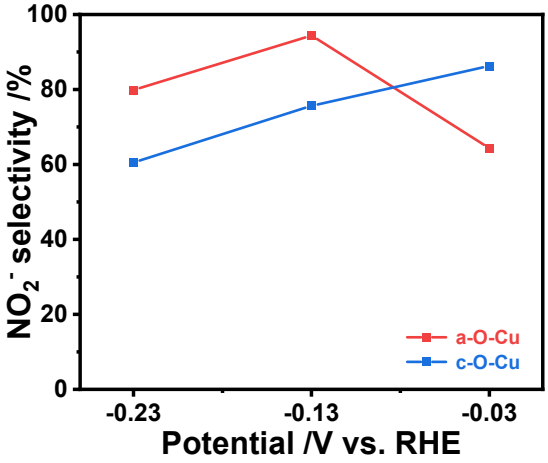

Figure S7. NO_2^- selectivity of a-O-Cu and c-O-Cu at different potentials for 3 h.

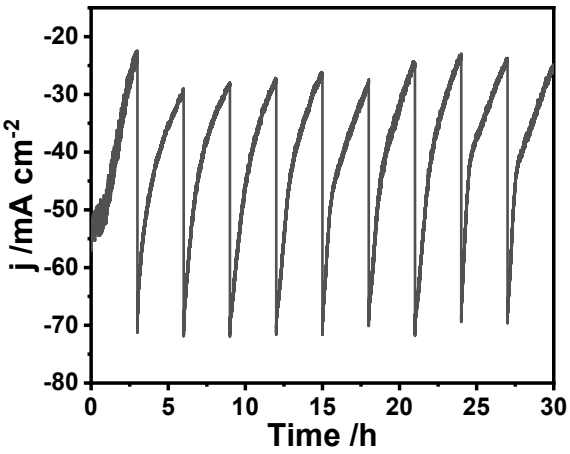

Figure S8. The i-t curves of a-O-Cu during ten consecutive cycling nitrate reduction into ammonia in 1 M KOH electrolyte with 200 ppm NO_3^- at -0.53 V vs. RHE. The first cycle involves the activation process of a-O-Cu, and thus its current density is smaller than that of the subsequent cycles, which shows almost the same current densities.

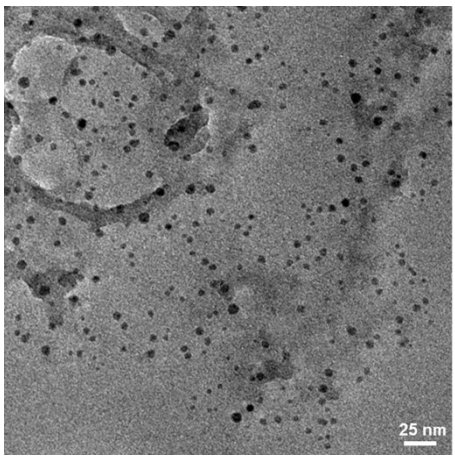

Figure S9. The TEM image of a-O-Cu after the electrochemical stability test.

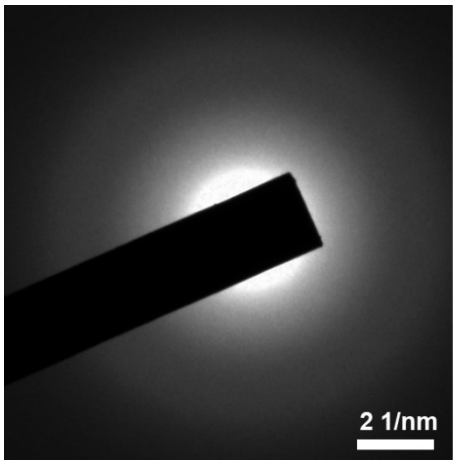

Figure S10. The corresponding SAED pattern of a-O-Cu after the electrochemical stability test.

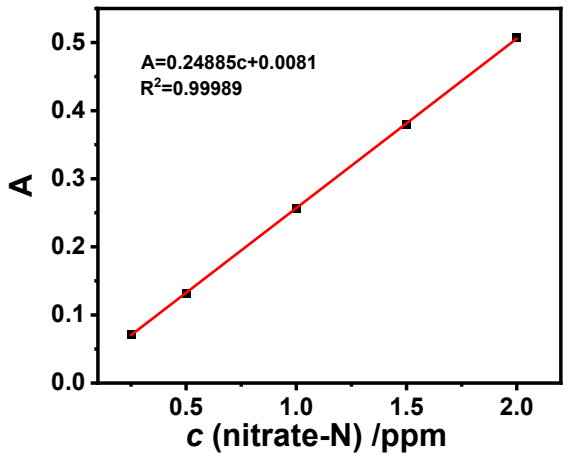

Figure S11. The UV-Vis absorption spectra corresponding calibration curves of NO_3^--N for NO_3^- electroreduction measurements by using ultrapure water as background solution.

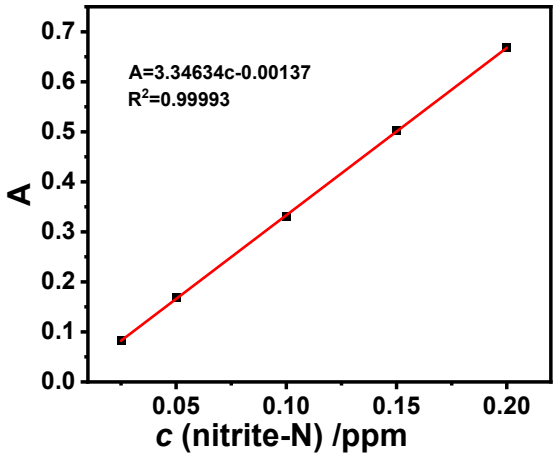

Figure S12. The UV-Vis absorption spectra corresponding calibration curves of NO_2^--N for NO_3^- electroreduction measurements by using ultrapure water as background solution.

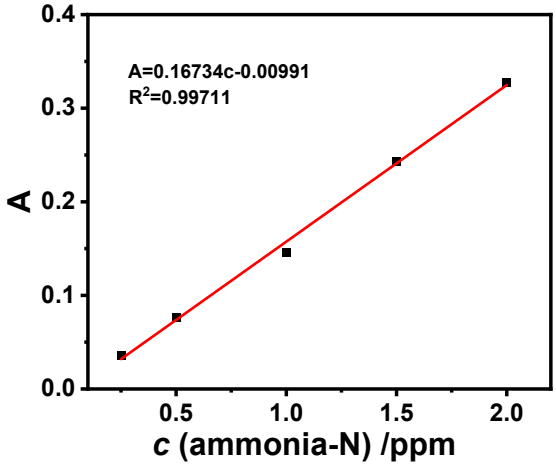

Figure S13. The UV-Vis absorption spectra corresponding calibration curves of NH_4^+-N for NO_3^- electroreduction measurements by using ultrapure water as background solution.

Figure S14. The typical H-type electrochemical cell separated by a Nafion 117 membrane.

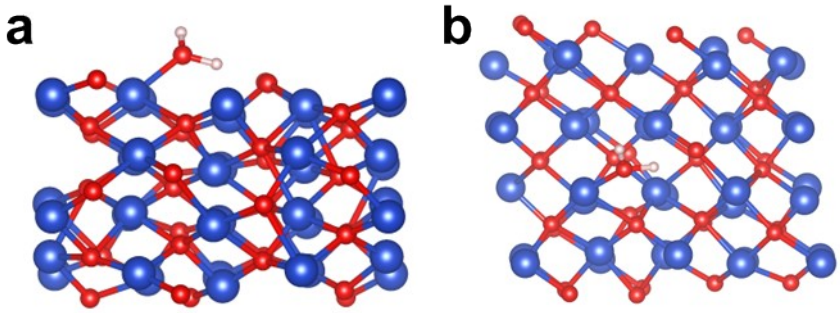

Figure S15. (a) The side view and (b) corresponding top view of atomic structure of *H_2O on a-O-Cu.

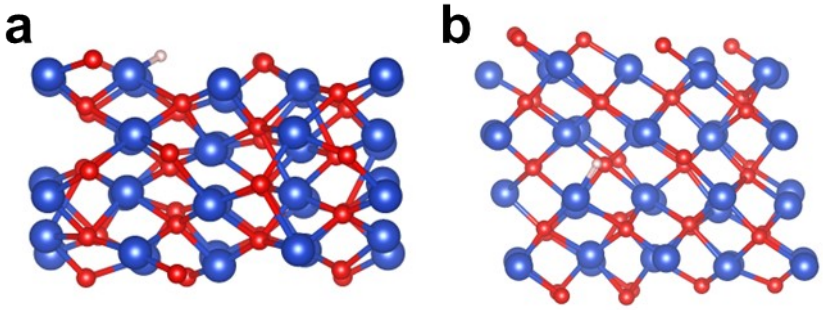

Figure S16. (a) The side view and (b) corresponding top view of atomic structure of *H on a-O-Cu.

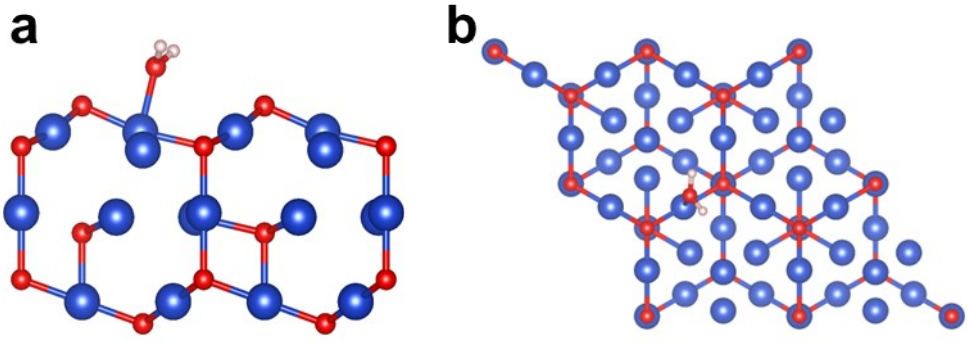

Figure S17. (a) The side view and (b) corresponding top view of atomic structure of *H_2O on c-O-Cu (111).

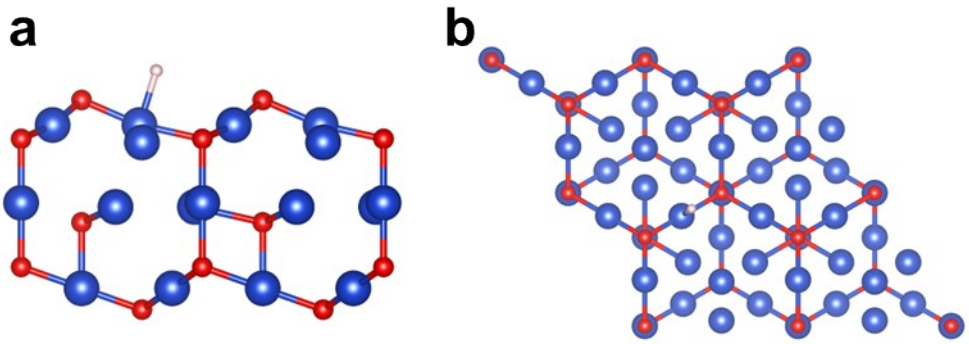

Figure S18. (a) The side view and (b) corresponding top view of atomic structure of *H on c-O-Cu (111).

Table S1. Performance comparison of our catalyst and the reported Cu-based catalysts in NO_3RR.

Catalysts	Electrolyte	Applied potential vs. RHE / V	NH_3 selectivity / %	FE / %	Yield rate of NH_3 / mmol h^{-1} cm^{-2}	Reference
a-O-Cu	200 ppm NO_3^--N + 1 M KOH	-0.53	93.6	84.9	0.14	This work
c-O-Cu	200 ppm NO_3^--N + 1 M KOH	-0.53	83.3	67.8	0.10	This work
CuPd@DCL-MCS	100 ppm NO_3^--N + 0.1 M Na_2SO_4	-1.35	5	36	/	Ref.7
Cu-N-C-800	50 ppm NO_3^--N + 0.05 M Na_2SO_4	-0.65	80.5	19.5	/	Ref.8
Plain Cu	200 ppm NO_3^--N + 0.1 M Na_2SO_4	-0.74	64.5	40.9	0.02	Ref.9
Cu/Cu_2O	0.05 M KNO_3 + 0.5 M Na_2SO_4	-0.8	83.3	58.1	/	Ref.10

Cu/Ni	50 ppm NO_3^--N + 0.1 M Na_2SO_4	-1.1	89.1	70	/	Ref.11
Cu-SAC	50 ppm NO_3^--N + 0.05 M Na_2SO_4	-1.06	81	46.7	0.034	Ref.8
Cu-Pd plate	135.5 ppm NO_3^--N	-1.1	35	35	/	Ref.12
Cu Nanobelt	30 ppm NO_3^--N + 0.05 M Na_2SO_4	-0.44	90	40	/	Ref.13

Reference

1. G. Kresse and J. Furthmüller, *Comp. Mater. Sci.*, 1996, **6**, 15-50.
2. G. Kresse and J. Furthmüller, *Phys. Rev. B*, 1996, **54**, 11169-11186.
3. J. P. Perdew, K. Burke and M. Ernzerhof, *Phys. Rev. Lett.*, 1996, **77**, 3865-3868.
4. G. Kresse and D. Joubert, *Phys. Rev. B*, 1999, **59**, 1758-1775.
5. P. E. Blöchl, *Phys. Rev. B*, 1994, **50**, 17953-17979.
6. H. Wang, R. Wei, X. Li, X. Ma, X. Hao and G. Guan, *J. Mater. Sci. Technol.*, 2021, **68**, 191-198.
7. H. Xu, J. Wu, W. Luo, Q. Li, W. Zhang and J. Yang, *Small*, 2020, **16**, 2001775.
8. T. Zhu, Q. Chen, P. Liao, W. Duan, S. Liang, Z. Yan and C. Feng, *Small*, 2020, **16**, 2004526.
9. C. Wang, Z. Liu, T. Hu, J. Li, L. Dong, F. Du, C. Li and C. Guo, *ChemSusChem*, 2021, **14**, 1825-1829.
10. C. Wang, F. Ye, J. Shen, K. H. Xue, Y. Zhu and C. Li, *ACS Appl. Mater. Interfaces*, 2022, **14**, 6680-6688.
11. J. Ding, W. Li, Q.-L. Zhao, K. Wang, Z. Zheng and Y.-Z. Gao, *Chem. Eng. J.*, 2015, **271**,

252-259.

12. T. F. Beltrame, M. C. S. Gomes, L. Marder, F. A. Marchesini, M. A. Ulla and A. M. Bernardes, *J. Water Process. Eng.*, 2020, **35**, 101189.

13. X. Wang, M. Zhu, G. Zeng, X. Liu, C. Fang and C. Li, *Nanoscale*, 2020, **12**, 9385-9391.